Experimental study of fast fission and quasifission in the ^{40}Ca $+$ ^{208}Pb reaction leading to the formation of the transfermium nucleus ^{248}No

E. M. Kozulin[1,2] G. N. Knyazheva[1,2] A. A. Bogachev[1] V. V. Saiko[1,3] A. V. Karpov[1,2]
I. M. Itkis[1] K. V. Novikov[1,2] Y. S. Mukhamejanov[1,3,4] I. V. Pchelintsev[1] I. V. Vorobiev,[1]
T. Banerjee[1] M. Cheralu,[1] and Pushpendra P. Singh[5]

[1]*Flerov Laboratory of Nuclear Reactions, Joint Institute for Nuclear Research, 141980 Dubna, Russia*
[2]*Dubna State University, 141980 Dubna, Russia*
[3]*Institute of Nuclear Physics, Almaty, 050032 Kazakhstan*
[4]*Al-Farabi Kazakh National University, Almaty, 050040 Kazakhstan*
[5]*Department of Physics, Indian Institute of Technology Ropar, Rupnagar, Punjab 140001, India*

Background: The stability of the transfermium nucleus against fission is mainly determined by the shell correction depending on its angular momentum and excitation energy.

Purpose: The study of the fast fission process of the transfermium nucleus ^{248}No and its dependence on the interaction energy and introduced angular momentum.

Methods: Mass-energy distributions of the ^{248}No fission fragments formed in the ^{40}Ca $+$ ^{208}Pb reaction at energies above the Coulomb barrier have been measured using the double-arm time-of-flight spectrometer CORSET at the ^{40}Ca-beam energies of 223, 250, and 284 MeV.

Results: The contribution of the fast fission process is determined from the calculations of the driving potential, taking into account shell effects and rotational energy and amounts to 39% and 61% at 250 and 284 MeV, respectively. The mass-energy distributions of the quasifission and fast fission fragments have been extracted by subtracting the mass-energy matrices associated with compound nucleus fission from those of all measured fissionlike events. The asymmetric fragments with masses 97 and 151 u were found to be the most probable in the fast fission of ^{248}No. With increasing ^{40}Ca energy from 250 to 284 MeV the mass distributions of the fast fission fragments change slightly.

Conclusions: Contrary to quasifission in which the fragments are focused mainly around the closed neutron or proton shells, the influence of known proton or neutron shells on the asymmetric mass distribution in the fast fission process was not observed.

I. INTRODUCTION

The fusion of heavy nuclei is a complex process in which a total rearrangement of the colliding nuclei structure occurs and they lose completely their individuality forming an excited compound nucleus (CN). Interest to fusion reactions has not waned for many years since this process is one of the ways to synthesize and study the properties of nuclei. At present the complete fusion reactions is the only "working" method for producing the superheavy elements [1].

In the interaction of heavy nuclei, the complete fusion process competes with other possible reaction channels, such as deep inelastic scattering, quasifission, and fast fission [2]. The separation of various processes from the total reaction cross section is a long-standing and extremely important task in the physics of nuclear reactions with heavy ions. In the past two decades significant progress was achieved in solving this problem experimentally and theoretically [3–6]. The total cross section of all reaction channels characterized by large energy dissipation and nucleon transfer is usually divided into the cross section of deep inelastic collisions and the capture cross section. The capture process is possible only when the introduced angular momentum l is lower than the critical value L_{cr} at which the interaction energy is equal to the effective barrier defined as a sum of the interaction barrier and centrifugal energy of the system [2].

The compound nucleus has an excitation energy defined as $E_{CN}^* = E_{c.m.} + Q_{CN}$, where $E_{c.m.}$ is the energy in the center-of-mass (c.m.) system, Q_{CN} is the mass difference of the formed CN and the interacting nuclei. The excited CN can undergo fission or cool down due to the evaporation of light particles (neutrons, protons, and α particles) and the emission of γ quanta. Thus, the fusion cross section is the sum of the evaporation residues (ERs) formation cross section σ_{ER}, i.e., the process in which the nucleus survives against fission, and the fission cross section σ_{fis}. The competition between survival and fission processes is determined, first of all, by the difference between the fission barrier B_f and the neutron binding energy B_n. In the reactions with heavy ions, the introduced angular momentum can reach quite large values of $\sim$100$\hbar$

that significantly impacts the fission barrier of the composite system since it consists of a liquid-drop fission barrier B_f^{LDM}, shell correction δU, and the difference ΔE_{rot} between the rotational energies at the barrier and in the ground state,

$$B_f = B_f^{\mathrm{LDM}} - \delta U + \Delta E_{\mathrm{rot}}. \qquad (1)$$

Since the moment of inertia of the nucleus in the ground state is less than at the barrier (saddle point), the value $\Delta E_{\mathrm{rot}} = \hbar^2 l(l+1)(1/2\Im_{\mathrm{sp}} - 1/2\Im_{\mathrm{gs}})$ is negative, where l is the angular momentum of the nucleus and $\Im_{\mathrm{SP}}$ and $\Im_{\mathrm{gs}}$ are the moments of inertia of the nucleus at the saddle point and the ground state, respectively. Thus, the fission barrier decreases with increasing the angular momentum. When a certain value of the angular momentum $L_{Bf=0}$ is reached, the fission barrier completely disappears. In this case, the trap to hold the formed composite system does not exist, and it immediately goes into the fission channel. This process, which takes place at angular momenta in the range of $L_{Bf=0} < l < L_{\mathrm{cr}}$ is commonly called fast fission.

The process of fast fission was studied both experimentally and theoretically [7–14]. The main attention in these investigations was paid to the compound nuclei with a sufficiently large liquid-drop fission barrier. For such nuclei, the conditions for the fast fission to occur can be calculated using the rotating liquid-drop model (LDM) [15].

As known, for transfermium elements the liquid-drop fission barrier approaches zero, and the stability of the nucleus relative to fission is mainly determined by the shell correction. With increasing the CN excitation energy, temperature effects become important in the driving potential, trying to bring the fission barrier closer to its liquid-drop limit. This additional temperature factor should be especially pronounced in the region of the heaviest nuclei and lead to an increase in the contribution of fast fission to the capture cross section. The study of the influence of angular momentum l and CN excitation energy on the height of the fission barrier of transfermium elements is very important for experiments on the synthesis of superheavy elements.

The fast fission phenomenon in the region of the heaviest nuclei remains insufficiently studied. For example, in Ref. [13], three systems Ar + Au, Ar + Bi, and Ar + U are considered and compared with the predictions of static and dynamic models. For the two lighter systems, the fast fission was observed only at angular momenta higher than $L_{Bf=0}$, whereas for the heaviest one it was observed in the entire range of interaction energies. In Ref. [16] the fast fission was investigated for the Cl + Au reaction. The authors found that the width of the symmetric component of the mass distribution strongly increases with increasing L_{cr}, which is associated with the disappearance of the fission barrier. The properties of the fast fission fragments of ^{250}Cf were studied radiochemically in the ^{12}C + ^{238}U reaction [17]. Experimental mass distributions of fissionlike fragments were measured at the incident energies below and above the fast fission threshold. An asymmetric component with the mass asymmetry $\eta = (M_{\mathrm{H}} - M_{\mathrm{L}})/(M_{\mathrm{H}} + M_{\mathrm{L}}) \approx 0.22$ in the mass distribution was found. The authors associated this component with the manifestation of the fast fission process.

It should be noted that in the reactions leading to the formation of transfermium elements, the contribution of the quasifission (QF) process also becomes significant. The properties of fragments formed in the CN fission, QF, and fast fission processes are quite similar, and experimental separation of these channels is a difficult task. Fast fission becomes possible only at energies above the threshold determined from the angular momentum condition $L_{Bf=0} < L_{\mathrm{cr}}$. QF has the maximum contribution to the capture cross section at energies near the Coulomb barrier, and it decreases with increasing the interacting energy [3]. Contrary to fast fission, there is no specific angular momentum range for the appearance of the QF process.

The aim of this paper is to study experimentally the fast fission process in ^{40}Ca + ^{208}Pb reaction at energies above the Coulomb barrier. The fission barrier of ^{248}No formed in this reaction is almost entirely defined by shell correction. In this investigation the mass-energy distributions of fragments were measured at an energy below the threshold for the fast fission process ($E_{\mathrm{lab}} = 223$ MeV) and at two energies ($E_{\mathrm{lab}} = 250$ and 284 MeV) above the threshold. In addition, the mass-energy distributions of the CN-fission and QF fragments for the similar reactions ^{44}Ca + ^{206}Pb and ^{48}Ca + ^{208}Pb were studied earlier [18,19]. Mass-angular distributions for ^{40,48}Ca + ^{208}Pb were also studied in Refs. [20–22]. This information made it possible to extract the fast fission events formed in the ^{40}Ca + ^{208}Pb reaction and to study in detail the properties of the fragment mass-energy distributions for this process.

II. FISSION, QUASIFISSION, AND FAST FISSION IN THE ^{40}Ca + ^{208}Pb REACTION

Both interacting partners of the reaction under study are double magic nuclei. Contrary to the reactions with deformed nuclei, in this case only a compact configuration between magic spherical nuclei in the entrance channel is possible. However, the Coulomb factor $Z_1 Z_2 = 1640$, which leads to a significant Coulomb repulsion between the interacting nuclei after their contact and suppression of the formation of ^{248}No compound nucleus by a competing QF process. Measurements of the mass-angular distributions of the ^{40}Ca + ^{208}Pb reaction fragments performed in Ref. [20] revealed the presence of an asymmetric component in the "forward-backward" direction, typical for the QF process, as well as the component expected for the CN fission.

The key parameter used to estimate the probability of QF is the mean fissility parameter x_{m}, which was determined from the analysis of a large set of experimental data on the mass-angular distributions of fragments in the reactions with heavy ions [23]. It is defined as $x_{\mathrm{m}} = 0.75 x_{\mathrm{eff}} + 0.25 x_{\mathrm{CN}}$, where x_{CN} is the fissility parameter for CN, and x_{eff} is the effective fissility parameter [24], reflecting the entrance-channel charge and mass asymmetry.

From the analysis of experimental ER cross sections, the fusion probabilities for cold fusion reactions have been estimated [4]. The values of P_0 calculated at the excitation energy $E^* = 40$ MeV (significantly higher than the barriers for cold fusion) were described by the Fermi function depending on
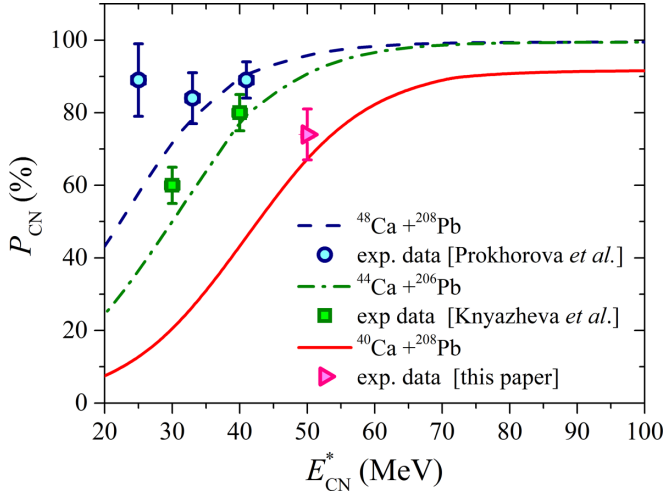
FIG. 1. The fusion probability (lines) as a function of the excitation energy of the compound nuclei formed in the $^{40}Ca + ^{208}Pb$, $^{48}Ca + ^{208}Pb$, and $^{44}Ca + ^{206}Pb$ reactions, calculated using Eqs. (2) and (3). The circles and the squares are the experimentally estimated fusion probabilities for the $^{48}Ca + ^{208}Pb$ [19] and $^{44}Ca + ^{206}Pb$ [18] reactions.

the mean fissility parameter x_m [25],

$$P_0 = \frac{1}{1 + \exp\left[\frac{x_m - 0.776}{0.0067}\right]}. \tag{2}$$

The fusion probability also depends on the interaction energy [4],

$$P_{CN}(E^*, l) = \frac{P_0}{1 + \exp\left[\frac{E_B^* - E_{int}^*(l)}{\Delta}\right]}, \tag{3}$$

where E_B^* is the excitation energy of the CN at the beam energy in the c.m. system equal to the Bass barrier [24], $E_{int}^*(l) = E_{c.m.} + Q - E_{rot}(l)$ is the "internal" excitation energy, which also determines the attenuation of the shell correction to the fission barrier of the CN; Δ is the adjustable parameter.

Figure 1 shows the dependence of the fusion probability on the CN excitation energy calculated using Eqs. (2) and (3) for the reaction under study as well as for the similar systems $^{44}Ca + ^{206}Pb$ and $^{48}Ca + ^{208}Pb$ for which the fusion probability was obtained from the analysis of mass energy and angular distributions [18,19]. The experimentally estimated probabilities agree well with the dependence proposed by Zagrebaev and Greiner [4]. Despite the Coulomb factor of these three reactions is the same, the mean fissility parameter is different: $x_m = 0.723$ for the $^{48}Ca + ^{208}Pb$ reaction, 0.741 for $^{44}Ca + ^{206}Pb$, and 0.759 for $^{40}Ca + ^{208}Pb$. The contribution of the QF process increases with an increase in the mean fissility parameter.

The experimentally estimated values of P_{CN} are in agreement with the calculated results, except the lowest-energy point for $^{48}Ca + ^{208}Pb$ [19] at which the experimental value is two times higher than the calculated one. The mass-angular distributions of binary fragments formed in the $^{40,44,48}Ca + ^{204,208}Pb$ reactions measured by ANU group [20]

also indicate the lower contribution of the QF process in the $^{48}Ca + ^{208}Pb$ reaction at energies near the Coulomb barrier. It was supposed that the QF yield depends on the number of neutron and proton shells in the reaction entrance channel: the more magic numbers, the higher the probability of a complete fusion of the nuclei. However, this does not explain such a large difference in the contributions of the QF process in the $^{40,48}Ca + ^{208}Pb$ reactions since in both reactions all the partners are doubly magic nuclei. The difference between ^{48}Ca and ^{40}Ca is in the presence of a neutron skin in the case of ^{48}Ca. For this nucleus the r_n-r_p is about 0.14–0.20 fm (for ^{40}Ca it is about zero) [26,27]. The neutron skin changes the balance between the nuclear and the Coulomb forces in the entrance channel and may lead to an increase in the fusion probability. Note that the heaviest superheavy elements were produced in the reactions with neutron-rich ^{48}Ca. The influence of the neutron skin on the nuclear interaction mechanism is expected to be more pronounced at the near-barrier energies where the minimal contribution of the QF was found. With increasing incident energy, the effect of the skin decreases and the QF contribution increases. For the reaction with ^{48}Ca [21] at energies above the barrier the forward-backward asymmetric QF component appears in the mass-angular distributions similarly to the ^{40}Ca-induced reaction.

Figure 1 shows that as expected the probability of fusion decreases at the transition from $^{48}Ca + ^{208}Pb$ to $^{44}Ca + ^{206}Pb$. Thus, to estimate the QF cross section in the $^{40}Ca + ^{208}Pb$ reaction we can use the following relation:

$$\sigma_{QF} = \sigma_{cap}[1 - P_{CN}(E_{c.m.}, l)]. \tag{4}$$

The capture cross sections, partial cross sections, and critical angular momenta L_{cr} were calculated using the code of coupling channel model KANTBP [28]. The advantage of this code, compared to the widely used codes of NRV [29,30] and CCFULL [31], is the careful treating of boundary conditions for solving the set of coupled Schrödinger equations. It allows one to keep a high accuracy of calculations that take into account a large number of coupled channels.

The ER cross section in the studied reaction is expected to be several orders of magnitude smaller than the cross section of the CN fission [32], so this process was not considered in this analysis.

Since the fission barrier of ^{248}No is determined mainly by the shell correction, the angular momentum must be calculated taking into account the influence of the CN temperature on the value of δU. The dependence of the fission barrier height on the temperature and angular momentum was determined in the calculations of the driving potential taking into account shell effects and rotational energy as

$$F(q, T, l) = V_{mac\text{-}mic}(q) + E_{rot}(q, l) - a(q)T^2, \tag{5}$$

where $V_{mac\text{-}mic}(q)$ is the macroscopic-microscopic potential, T is the nuclear temperature, $a(q)$ is the level-density parameter [33], and q is a set of collective degrees of freedom of the system. Rotational energy $E_{rot}(q, l) = \hbar^2 l(l + 1)/2\mathfrak{J}_\perp(q)$, where $\mathfrak{J}_\perp(q)$ is a rigid body moment of inertia.

TABLE I. The properties of the ^{40}Ca + ^{208}Pb reaction: E_{lab} is the bombarding energy in the laboratory system, $E_{c.m.}/E_B$ is the ratio of energy in the c.m. frame to the Bass barrier [24], E^* is the initial excitation energy of the formed CN, L_{cr} is the critical angular momentum, $L_{Bf=0}$ is the angular momentum at which the fission barrier disappears, the capture σ_{cap}, QF σ_{QF}, CN-fission σ_{fis}, and fast fission σ_{fast} cross sections calculated with the KANTBP code [28].

E_{lab} (MeV)	$E_{c.m.}/E_B$	E^* (MeV)	L_{cr} $\hbar$	$L_{Bf=0}$ $\hbar$	σ_{cap} (mb)	σ_{QF} (mb)	σ_{fis} (mb)	σ_{fast} (mb)	$\sigma_{fis}/\sigma_{cap}$ (%)	σ_{QF}/σ_{cap} (%)
223	1.03	49	62	63	212	53	159	0	75	25.0
250	1.16	73	94	62	620	62	305	253	49	10.0
284	1.58	101	113	61	931	79	280	572	30	8.5

The potential energy $V_{mac-mic}(q)$ is calculated using a macroscopic-microscopic approach [34] based on a two-center shell model [35]. In this approach, nuclear forms are described by five collective degrees of freedom q: the relative distance between the centers of fragments r, the ellipsoidal deformations of each fragment $\delta_{1,2}$, the mass asymmetry η, and the neck parameter ε. To simplify the calculations, we used mirror-symmetric shapes of fragments ($\eta = 0$, $\delta_1 = \delta_2 = \delta$). We used the value of $\varepsilon = 0.35$, recommended in Ref. [36] for the fission process. Thus, the potential and free-energy surfaces were calculated for the variable shape parameters: relative distance r and ellipsoidal deformation δ.

The nuclear temperature and the angular momentum are included in the expression for the driving potential (5) as parameters. The constant value of T is determined from the excitation energy E^* of a rotating compound nucleus in the ground state, according to the Fermi-gas model: $T = [E^*/a(q)]^{1/2}$. The value of the angular momentum $L_{Bf=0}$ at which the fission barrier disappears was determined from the condition, $\frac{\partial F}{\partial q}(q, T, L_{Bf=0})|_T = \frac{\partial^2 F}{\partial q^2}(q, T, L_{Bf=0})|_T = 0$.

The obtained values of $L_{Bf=0}$ for the ^{40}Ca + ^{208}Pb reaction are presented in Table I. The fast fission cross sections for different energies of the projectiles were determined as the sum of the partial waves of the fusion cross section in the corresponding range of angular momenta $L_{Bf=0} < l < L_{cr}$. The capture cross sections as a function of the introduced angular momentum for the reaction under study, calculated using the coupled channels model, are shown in Fig. 2.

III. EXPERIMENT

The measurements were carried out using the U400 cyclotron at the Flerov Laboratory of Nuclear Reactions, Dubna, Russia. The 250-μg/cm^2 ^{208}Pb target deposited on 50-μg/cm^2 carbon backing was irradiated with the 223-, 250-, and 284-MeV ^{40}Ca beam. The target backing faced the beam. The energy resolution was about 1%. Beam intensities on targets were 1 to 2 pnA. The enrichment of the ^{208}Pb target was 99.2%.

The binary reaction products were measured in coincidence by the double-arm time-of-flight spectrometer CORSET [37]. Each arm of the spectrometer consists of a compact start detector and a position-sensitive stop detector based on microchannel plates. The angular acceptance of the

spectrometer arms in the reaction plane was ±10º and ±19º for the first and the second arms, respectively. The spectrometer arms were positioned at the angles 55º and 61º–67º with respect to the beam axes. This geometry allows us to measure the coinciding fragments within the mass ratio from 0.4 to 4. The position resolution of the stop detectors was 0.3º, and the time resolution was about 200 ps. The mass and energy resolutions of the CORSET setup were deduced from the full width at half maximum of the mass and energy spectra of elastically scattered particles, respectively. The mass resolution of the spectrometer under these conditions was ±2 u.

Data processing assumed standard two-body kinematics [37]. Primary masses, velocities, energies, and angles of reaction products in the c.m. system were calculated from the measured velocities and angles using the momentum and mass conservation laws, assuming that the mass of the composite system is equal to $M_{target} + M_{projectile}$. Corrections for fragment energy losses in the target material and the foils of detectors were taken into account. The extraction of the binary reaction channels exhibiting full momentum transfer was based on the analysis of the kinematical diagram (see Refs. [37,38] for details).
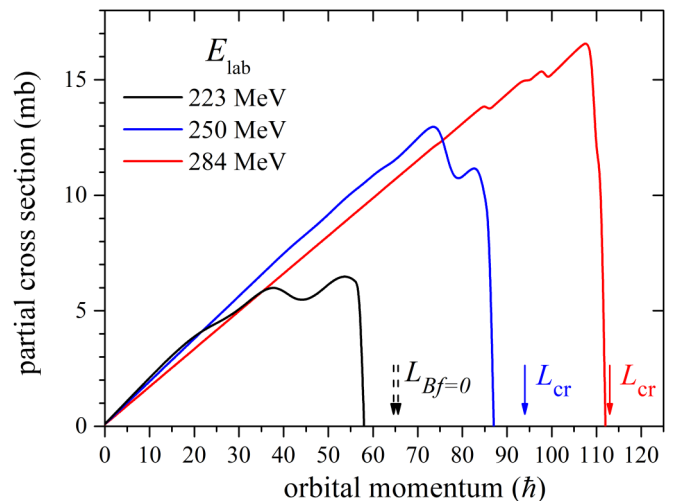

FIG. 2. Partial capture cross sections as a function of angular momentum for the ^{40}Ca + ^{208}Pb reaction at the projectile energies of 223, 250, and 284 MeV, calculated within the coupled channels approach using the KANTBP code [28].
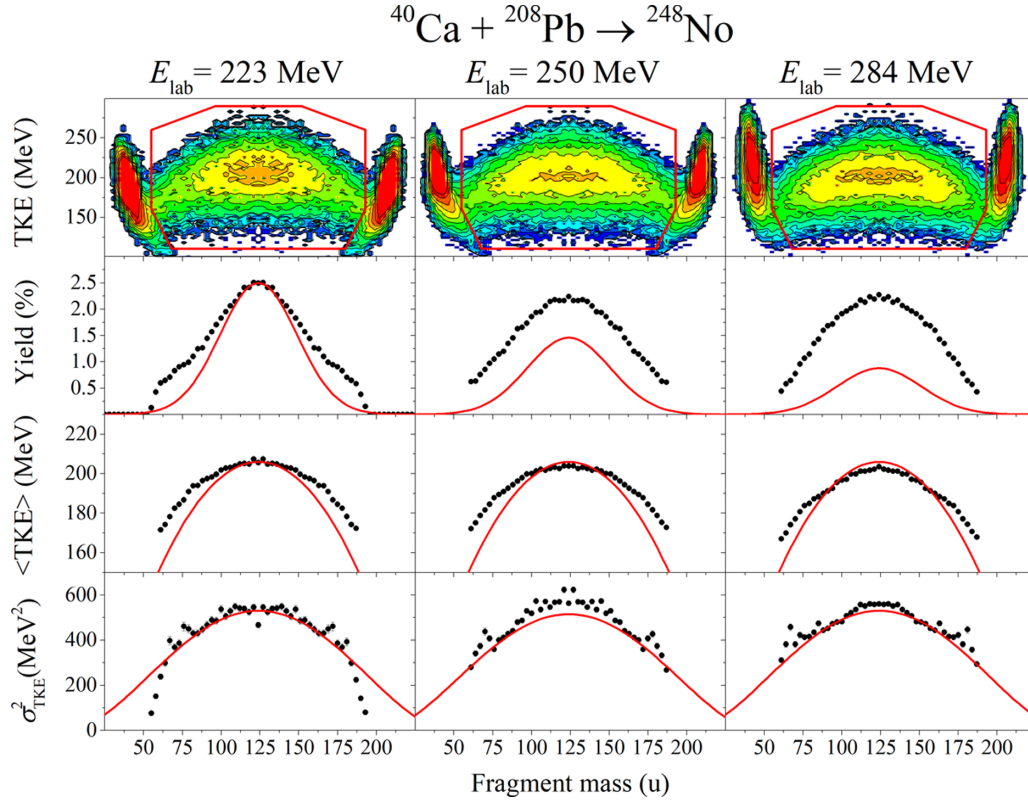
FIG. 3. The mass-energy distributions of binary fragments formed in the $^{40}Ca + {}^{208}Pb$ reaction at energies above the Coulomb barrier. From top to bottom: M-TKE matrices of all binary reaction products, mass yields, average total kinetic energies and their variances as a function of mass of fissionlike fragments inside contour lines on M-TKE matrices. The solid lines correspond to the expectation from the LDM.

IV. RESULTS

The mass-total kinetic energy (M-TKE) distributions of the primary binary fragments obtained in the $^{40}Ca + {}^{208}Pb$ reaction leading to the formation of ^{248}No at energies above the Coulomb barrier are shown in Fig. 3. In M-TKE matrices, reaction products with masses close to the masses of the projectile and target and with energies near $E_{c.m.}$ are associated with elastic and quasielastic events and can be fairly well separated from other reaction channels. Fissionlike products located between quasielastic peaks inside contour lines in the M-TKE distributions in Fig. 3 are characterized by large mass transfer and energy dissipation and can occur as a result of the CN fission as well as of fast fission and QF processes. The mass distributions normalized to 200%, the average total kinetic energies ⟨TKE⟩ and their variances σ^2_{TKE} of fissionlike fragments (events inside the contour lines in M-TKE distributions) are also shown in Fig. 3. The red lines delineate the dependences expected from the LDM for the $^{248}No^*$ fission fragments (see Sec. V A for details).

At the ^{40}Ca energy of 223 MeV, the angular momenta introduced into the composite system do not exceed the value at which the fission barrier vanishes (see Table I). At this energy, the CN-fission process is mainly observed with a noticeable contribution of QF in the region of asymmetric masses. At $E_{lab} = 250$ and 284 MeV, the fast fission process makes up a significant part of the capture. Table I shows the contributions of the CN fission in the measured mass-energy distributions of

all fissionlike fragments (the sum of the fission, QF, and fast fission processes).

It is seen from Fig. 3 that the mass-energy distributions of the fissionlike fragments change insignificantly whereas the yields of CN fission are less than 50% at the energies of 250 and 284 MeV. The average TKEs and their variances as a function of the fragment mass are similar for all measured energies. However, the mass distributions at the energies of 250 and 284 MeV cannot be described by a single Gaussian expected in accordance with the LDM, although at the energy of 223 MeV where fast fission is completely absent, the mass yield of symmetric fragments is well reproduced by a Gaussian. Deviations are detected only for asymmetric fragments. As was shown in Refs. [18,19] for similar systems formed in $^{48}Ca + {}^{208}Pb$ and $^{44}Ca + {}^{206}Pb$, these asymmetric fragments are formed mainly in the QF process.

V. ANALYSIS AND DISCUSSION

A. Fission properties of the excited ^{248}No

It is known that the fragments mass distributions of spontaneous fission of transfermium nobelium isotopes vary from asymmetric with a heavy fragment mass near 140–144 u to narrow symmetric. The transition between asymmetric and symmetric division occurs around ^{256}No [39]. With an increase in the excitation energy of the fissioning nucleus, the contribution of symmetric fission inherent in the LDM increases, and the influence of the shell effects responsible for
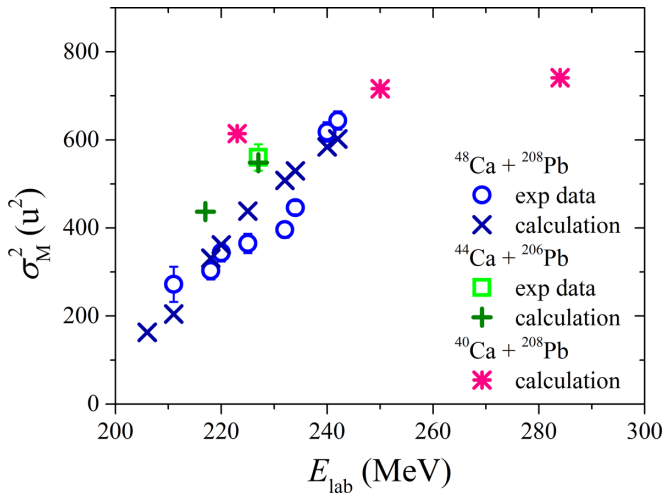
FIG. 4. The variances of mass distributions of the ^{248,250,256}No fission fragments obtained in the ^{40}Ca + ^{208}Pb, ^{44}Ca + ^{206}Pb, and ^{48}Ca + ^{208}Pb reactions as a function of the Ca-ions energy. The experimental points for ^{44}Ca + ^{206}Pb (squares) and ^{48}Ca + ^{208}Pb (circles) are taken from Refs. [18,19]. The values calculated using Eq. (6) are shown by crosses and stars.

asymmetric fission decreases exponentially [3]. For example, the mass distribution of ^{250}No fission fragments formed in the ^{44}Ca + ^{206}Pb reaction at the excitation energy of 30 MeV has a pronounced asymmetric component, and at the excitation energy of 40 MeV this component almost disappears and the fission of this nucleus is symmetric [18].

As can be seen from Table I, the initial (without taking into account the rotational energy) excitation energy of ^{248}No studied in this paper is quite high, being 49 to 101 MeV. It is expected that at these excitation energies the CN fission properties will be determined mainly by the liquid-drop component of the potential energy of the fissioning nucleus.

According to the LDM, the mass distribution of fragments is symmetric and has a Gaussian shape. Based on the analysis of a large set of experimental data on the mass and energy distributions of fission fragments of hot nuclei [40], it was shown that the variance of the LDM component increases linearly with the nucleus temperature at the saddle point T_{SP},

$$\sigma_M^2 = \frac{A_{CN}^2}{16} T_{SP} \left[\frac{d^2V}{d\eta^2} \right]^{-1} + 0.12\langle l^2 \rangle, \quad (6)$$

where A_{CN} is the mass of the CN, $\frac{d^2V}{d\eta^2}$ is the rigidity of the fissionning nucleus depending on the fissility parameter. For ^{248,250}No $\frac{d^2V}{d\eta^2} \approx 11$ and for ^{256}No $\frac{d^2V}{d\eta^2} \approx 14$ [40]. The experimental variances of the fission fragments mass distributions for ^{250,256}No isotopes formed in the ^{44}Ca + ^{206}Pb [18] and ^{48}Ca + ^{208}Pb [19] reactions together with the values estimated using Eq. (6) that depend on the Ca ions incident energy are shown in Fig. 4. It is seen that the calculated values are in a good agreement with the experimental data, and, consequently, Eq. (6) may be used to define the variances of the mass distributions of ^{248}No fission fragments formed in the ^{40}Ca + ^{208}Pb reaction.

According to the LDM suggested by Nix and Swiatecki in Ref. [41], the dependences of the average TKE and its variance on mass can be presented as

$$\langle \text{TKE} \rangle (M) = \text{TKE}_{A_{CN}/2} \{ 1 - (2M/A_{CN} - 1)^2 \}, \quad (7)$$

$$\frac{\langle \text{TKE} \rangle^2 (M)}{\sigma_{\text{TKE}}^2} = \text{const.} \quad (8)$$

The systematics obtained in Ref. [40] show that the variance of the fission-fragment energy distribution does not depend on the temperature of the fissioning nucleus but depends only on the introduced angular momentum l and Z_{CN}^2/A_{CN} parameter. Taking into account the energy resolution of the present measurements the variance of TKE distribution for ^{248}No may be estimated as

$$\sigma_{\text{TKE}}^2 = 480 + 0.018\langle l^2 \rangle. \quad (9)$$

The red lines in Fig. 3 correspond to the predicted LDM properties of the fission fragments of the excited ^{248}No nucleus calculated using the expressions (6)–(9): symmetric Gaussian-shape mass distribution with the variance estimated with Eq. (6), parabolic dependence of the $\langle \text{TKE} \rangle$ on fragment mass according to Eq. (7), and the TKE variance proportional to the $\langle \text{TKE} \rangle$ for a given fragment mass. Thus, the fission properties of the excited CN of ^{248}No are fairly well described by the relations (6)–(9) and can be used to simulate the mass-energy distributions of the fission fragments of ^{248}No (M-TKE)$_{\text{fis}}$ depending on the excitation energy and angular momentum of the fissioning nucleus.

B. Properties of the quasifission fragments

As already mentioned above at the ^{40}Ca incident energy of 223 MeV, the values of the critical angular momentum are less than $L_{Bf=0}$ (see Table I). Fissionlike fragments at this interaction energy are formed only in CN fission and QF. To extract the mass-energy distribution of QF fragments (M-TKE)$_{\text{QF}}$ from the experimental matrix of all fissionlike events (M-TKE)$_{\text{cap}}$, the simulated (M-TKE)$_{\text{fis}}$ matrix describing the properties of ^{248}No fission was subtracted

$$(M\text{-TKE})_{\text{QF}} = (M\text{-TKE})_{\text{cap}} - \frac{\sigma_{\text{fis}}}{\sigma_{\text{cap}}} (M\text{-TKE})_{\text{fis}}. \quad (10)$$

The total yields of matrices (M-TKE)$_{\text{cap}}$ and (M-TKE)$_{\text{fis}}$ were normalized to 200%.

The obtained mass-energy distribution is shown in Fig. 5. Also in this figure the mass distribution for the QF fragments formed in the ^{44}Ca + ^{206}Pb reaction, leading to the formation of a neighboring nucleus of ^{250}No from Ref. [18], is presented at the bombarding energies of 217 and 227 MeV. It should be noted that QF mass distributions for ^{44}Ca + ^{206}Pb change slightly with increasing the interaction energy from 217 to 227 MeV. At the same time, the yield of the QF into capture cross section decreases from 40% to 30%, respectively. The mass distribution for the QF fragments obtained in ^{48}Ca + ^{208}Pb at the beam energy of 232 MeV is also shown in Fig. 5 [19]. It is characterized by a narrower distribution.
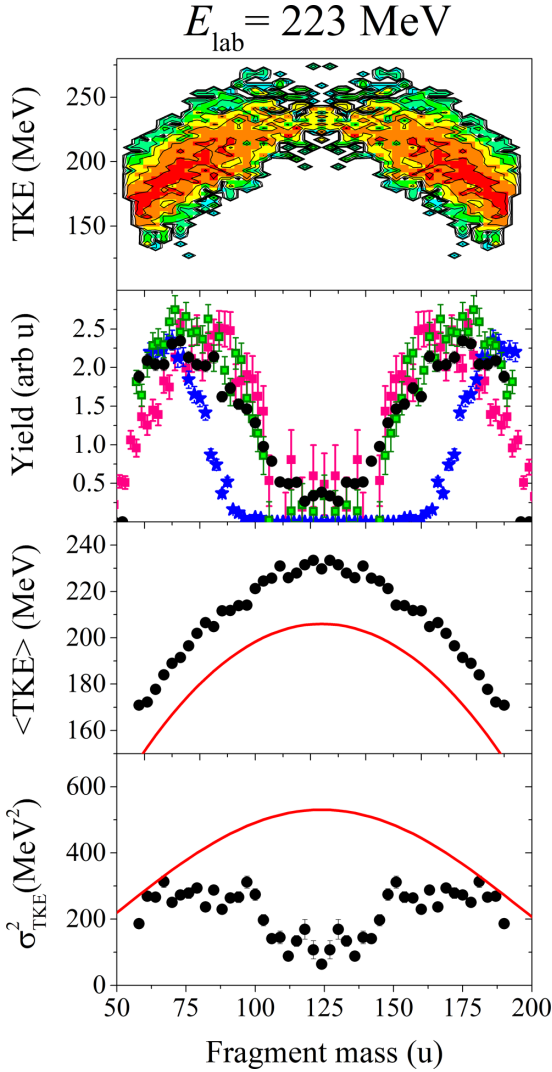
FIG. 5. The mass-energy distributions of extracted QF fragments formed in the ^{40}Ca $+$ ^{208}Pb reaction at $E_{\text{lab}} = 223$ MeV. From top to bottom: (M-TKE)$_{\text{QF}}$ matrix, mass yield, average total kinetic energy, and its variance as a function of mass. The mass distributions of QF fragments of ^{250}No formed in the ^{44}Ca $+$ ^{206}Pb reaction [18] are shown by the red ($E_{\text{lab}} = 217$ MeV) and green ($E_{\text{lab}} = 227$ MeV) squares. The blue stars correspond to the mass distribution of ^{48}Ca $+$ ^{208}Pb at $E_{\text{lab}} = 232$ MeV from Ref. [19]. The red lines represent the average TKE and its variance expected from the LDM for ^{248}No and calculated using Eqs. (7)–(9).

The mass distributions for the ^{44}Ca $+$ ^{206}Pb and ^{40}Ca $+$ ^{208}Pb reactions are very similar and have a wide asymmetric two-humped shape with a light-fragment mass of about 77 u that corresponds to the mass asymmetry $\eta \approx 0.38$. The maximum yields are observed at masses in the vicinity of the closed proton $Z = 28$ and neutron $N = 50$ shells in a light fragment. The formation of fragments near the closed shells, even at high excitation energies, is a specific feature of the QF process [3].

The TKE of QF fragments formed in the ^{40}Ca $+$ ^{208}Pb reaction is about 15–20 MeV higher and has a smaller dispersion than CN fission (red lines in Fig. 5). The variance of TKE

is about 200–300 MeV^2, which is about 1.5 times less than that for the CN fission. A similar trend for TKE distributions of QF fragments was found in the ^{48}Ca $+$ ^{208}Pb reaction [19]. This behavior is also typical for QF fragments [3].

C. Properties of fast fission fragments

As already mentioned the fast fission in the ^{40}Ca $+$ ^{208}Pb reaction is observed at the energies of 250 and 284 MeV. As a result of subtracting the simulated fission matrices (M-TKE)$_{\text{fis}}$ from the distributions of fissionlike fragments (M-TKE)$_{\text{cap}}$, the matrices containing QF and fast fission events were obtained. Since it is possible to extract the QF process unambiguously only at $E_{\text{lab}} = 223$ MeV, we assumed that the mass-energy distributions of QF fragments change slightly with an increase of the interaction energy. This assumption is confirmed by the dependence of the QF-fragments mass distributions on the interaction energy in the ^{44}Ca $+$ ^{206}Pb reaction (see the previous section). Moreover, the contribution of the QF process is expected to be small at the energies of 250 and 284 MeV (see Table I), such an assumption should not introduce large errors in the obtained mass-energy distributions of fast fission fragments.

To extract the mass-energy distributions of fast fission fragments (M-TKE)$_{\text{fast}}$, a matrix subtraction procedure similar to the one used for (M-TKE)$_{\text{QF}}$ was applied

$$(M\text{-TKE})_{\text{fast}} = (M\text{-TKE})_{\text{cap}} - \frac{\sigma_{\text{fis}}}{\sigma_{\text{cap}}}(M\text{-TKE})_{\text{fis}}$$

$$- \frac{\sigma_{\text{QF}}}{\sigma_{\text{cap}}}(M\text{-TKE})_{\text{QF}}. \qquad (11)$$

The obtained distributions are shown in Fig. 6. The mass distributions deviate from a single Gaussian for both energies. The behavior of $\langle$TKE$\rangle$ and its variance σ^2_{TKE} also differs from the LDM expectations. At $E_{\text{lab}} = 250$ MeV the $\langle$TKE$\rangle$ is virtually does not change in the mass range from 96 up to 152 u and amounts to 198 MeV. The variance of TKE is about 800 MeV^2 for the symmetric fragments, which is significantly higher than the LDM predictions (red lines in Fig. 6). At $E_{\text{lab}} = 284$ MeV the dependence of $\langle$TKE$\rangle$ on fragment mass is parabolic, but it is lower than expected in the LDM approach. The σ^2_{TKE} at this incident energy is lower than that at $E_{\text{lab}} = 250$ MeV and is about 640 MeV^2 for the symmetric fragments.

Thus, despite the rather large differences in the reaction entrance channel (the interaction energy increases by 29 MeV, and the critical angular momentum increases by 19 $\hbar$), the mass-energy distributions of fast fission fragments at $E_{\text{lab}} = 250$ and 284 MeV change slightly.

This is more clearly seen in Fig. 7 where the mass distributions of fast fission fragments, normalized to 200%, for the two measured energies are shown together. The standard deviations of the mass distributions are almost the same being 30.8 and 29.7 u for energies 250 and 284 MeV, respectively.

These mass distributions are best described by the sum of three Gaussians: a symmetric and two asymmetric, centered on complementary masses. The decomposition into Gaussians is also shown in Fig. 7. The χ^2 of the three Gaussians decomposition is 1.1 for the energy of 250 MeV and 0.9 for
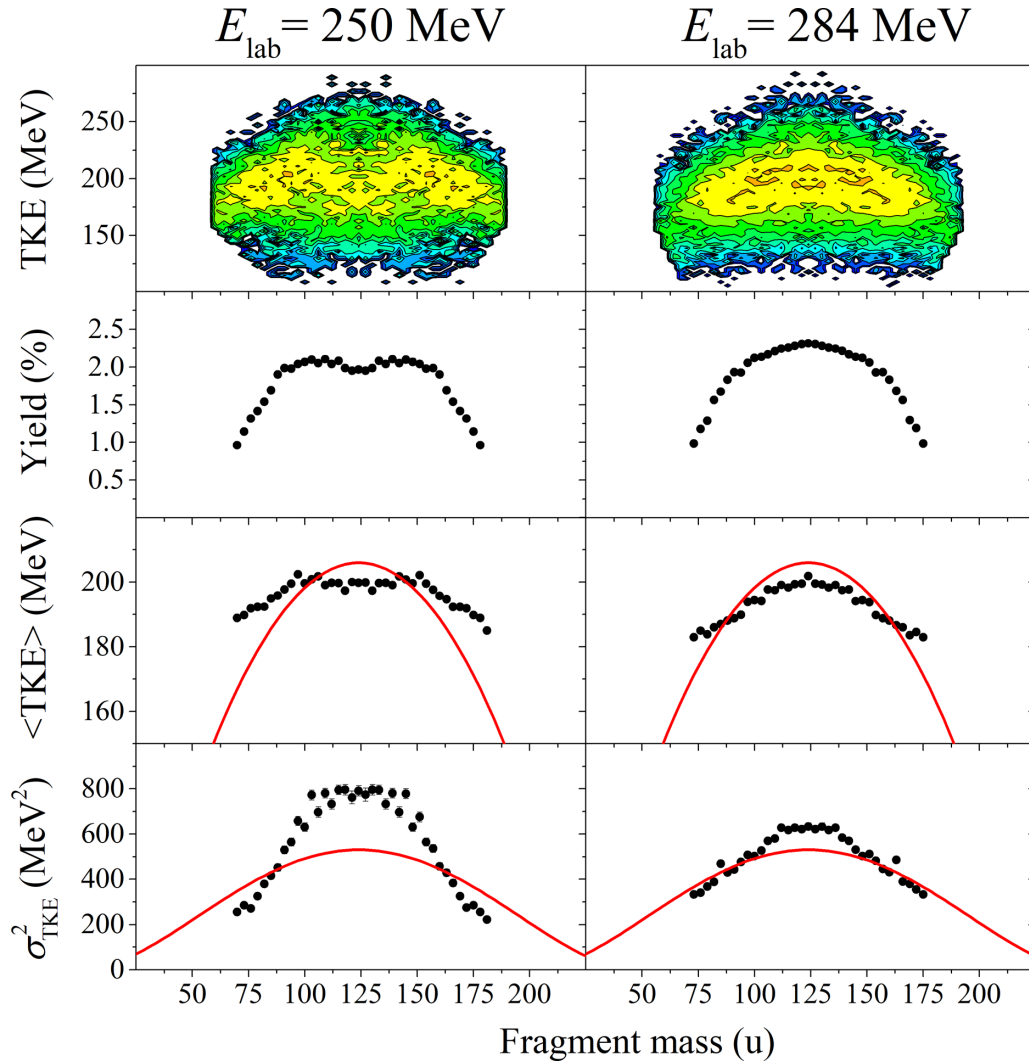
FIG. 6. From top to bottom: M-TKE distributions, mass yields, average TKEs and their variances as a function of mass for the fast fission fragments formed in the $^{40}\mathrm{Ca} + {}^{208}\mathrm{Pb}$ reaction at the incident energies of 250 and 284 MeV. The red lines delineate the LDM expectations.

284 MeV. A specific feature of the description of both distributions is that the positions of both asymmetric Gaussians have the same peak positions: 97 ± 2 and 151 ± 2 u. This mass ratio corresponds to the mass asymmetry $\eta \approx 0.218 \pm 0.015$. A very similar value of mass asymmetry of the fast fission fragments was obtained radiochemically for the $^{250}\mathrm{Cf}$ ($E^* \approx 100\,\mathrm{MeV}$) composite system formed in the $^{12}\mathrm{C} + {}^{238}\mathrm{U}$ reaction [17]. It is interesting to note that for $^{248}\mathrm{No}$ and $^{250}\mathrm{Cf}$ systems obtained in the different reactions with the different entrance-channel mass asymmetry, the asymmetry of the exit channel associated with the fast fission events turns out to be approximately the same.

In the case of the three-Gaussian description, the question about the origin and validity of the symmetric component arises. Probably, due to approximate model determination of the boundaries of different processes by the values of angular momenta, we could possibly underestimate the contribution of the CN fission in the symmetric mass region. And it also can be related with the contribution of QF which can populate the symmetric mass region with increasing interaction energy.

The similarity of the mass distributions regardless of the difference in the interaction energy of 29 MeV may indicate that the real excitation energy of the composite system at the scission point may be significantly lower for some reason. Despite the fast fission occurs in the short times of about 10^{-20}–10^{-21} s [9,12], there are experimental studies revealing the existence of prescission neutron emission [42]. This can also lead to a decrease in the excitation energy at the scission point and to "average" the mass distribution of fast fission fragments with respect to the composite system excitation energy at scission. For the studied reaction, the calculations of the scission-point rotational energy of the composite system consisting of the two formed fragments were made under the following assumptions: the fissioning system consists of two tangential spheroids rotating relative to the axis passing through their common center of mass and perpendicular to the fission one; the distance between their centers was determined from the $\langle\mathrm{TKE}\rangle$ measured experimentally in this paper. The values of the mean angular momenta of fast fission events $\langle l \rangle_{\mathrm{fast}}$ and average rotational energies E_{rot} for the bombarding
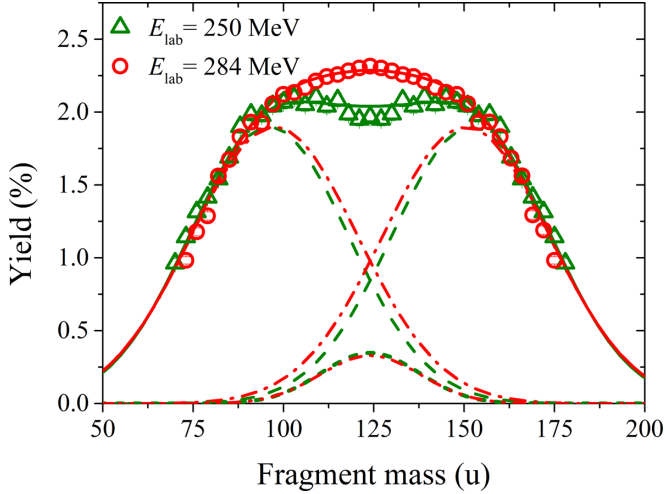
FIG. 7. Comparison of the mass distributions of fast fission fragments measured in the ^{40}Ca + ^{208}Pb reaction at the incident energies of 250 and 284 MeV. The lines show the description by Gaussians (see the text).

energies of 250 and 284 MeV are given in Table II. The values were calculated for the asymmetric and symmetric mass splits of the fast fission fragments. The results do not allow supposing that the excitation energy of the composite system at the scission point significantly changes due to the low rotation energy. In the fast fission process for the symmetric and asymmetric mass splits E_{rot} varies from 4.3 to 6.2 MeV. The average excitation energy of the composite system at scission E_{sc}^* is estimated as

$$E_{sc}^* = E_{c.m.} - Q - \text{TKE} - E_{rot} - E_{pre}, \qquad (12)$$

where $E_{c.m.}$ is the incident energy in the center-of-mass system, Q is the average Q value for entrance and exit channels, TKE is the total kinetic energy of both fragments measured experimentally in this paper, E_{rot} is the average rotational energy, and E_{pre} is the energy taken away by prescission neutrons.

The calculation of E_{pre} in the fast fission process is ambiguous. For CN fission the total number of neutrons emitted before scission $\bar{\nu}_{pre}$ may be estimated using the systematics

[40],

$$\bar{\nu}_{pre} = 1.98 - 0.0133A_{CN} - 0.0376E_{CN}^* + 0.00042A_{CN}E_{CN}^*. \qquad (13)$$

In CN fission the neutrons can be emitted before the saddle point as well as at the descent stage from saddle to scission [43]. In the fission of heavy actinides the descent stage takes rather long time (contrary to preactinide nuclei). According to Ref. [40], the number of neutrons emitted at the descent stage $\bar{\nu}_{pre}^{ss}$ can be estimated as

$$\bar{\nu}_{pre}^{ss} = \bar{\nu}_{pre}(1 - \exp\{-0.04329E_{CN}^* - 15.505x$$
$$+ 0.0456E_{CN}^*x + 11.904\}) \quad \text{for } x > 0.745, \qquad (14)$$

where x is the CN fissility parameter (for ^{248}No, $x = 0.873$). We may assume that the neutrons in the fast fission process can be emitted during the descent stage from the turning point to scission, and, consequently, $\bar{\nu}_{pre}^{ss}$ can be taken as the upper limit of prescission neutron multiplicity in the fast fission process. The estimated values of the energy taken away by prescission neutrons are given in Table II. It is seen that under this assumption, in the fast fission process, a significant part of the initial excitation energy is expended on neutron emission.

Despite the essential difference in the interaction energy of about 29 MeV, the excitation energy at scission for the fast fission fragments increases much less: by about 16 MeV for the asymmetric mass split and 9 MeV for the symmetric split (see Table II). Probably, this small difference is a reason (or one of the reasons) why the mass distributions of the fast fission events at these two incident energies are so similar. However, additional theoretical and experimental study on prescission neutron emission for the fast fission process is needed to make final conclusion.

VI. CONCLUSION

To study the influence of angular momentum and excitation energy introduced into the ^{248}No composite system on the reaction mechanism the mass and energy distributions of primary binary fragments formed in the ^{40}Ca + ^{208}Pb reaction at the incident energies of 223, 250, and 284 MeV were measured. The dependence of the fission barrier height on the temperature and the angular momentum was determined in the driving-potential calculations, taking into account shell effects and rotational energy. From these calculations, CN-fission and fast fission cross sections were obtained.

TABLE II. The properties of the fast fission fragments in dependence on the interaction energy: $\bar{\nu}_{pre}$ and $\bar{\nu}_{pre}^{ss}$ are the total number of prescission neutrons and the number of prescission neutrons emitted at descent stage from saddle to scission estimated using the systematics from Ref. [40], E_{pre} is the energy taken away by prescission neutrons, $\langle l \rangle_{fast}$ is the mean angular momentum for fast fission; TKE, E_{rot}, and E_{sc}^* are the average total kinetic energy, rotational energy, and excitation energy at scission for the symmetric ($A_{CN}/2 \pm 10$ u) and asymmetric ($M_L = 97 \pm 10$ u) fast fission fragments, formed in the ^{40}Ca + ^{208}Pb reaction.

E_{lab} (MeV)	$E_{c.m.}$ (MeV)	$\bar{\nu}_{pre}$	$\bar{\nu}_{pre}^{ss}$	E_{pre} (MeV)	$\langle l \rangle_{fast}$ $\hbar$	Asymmetric			Symmetric		
						TKE (MeV)	E_{rot} (MeV)	E_{sc}^* (MeV)	TKE (MeV)	E_{rot} (MeV)	E_{sc}^* (MeV)
250	209.7	3.5	3.0	30.9	74	199	4.4	72.1	199	4.3	88.1
284	238.2	5.4	4.7	48.2	88	193	5.9	88.2	199	6.2	97.5

The mass-energy distribution for the QF fragments was extracted from the measured distribution for all binary fragments at the incident energy of 223 MeV. The mass distribution is asymmetric and the mass asymmetry $\eta = (M_H - M_L)/(M_H + M_L) \approx 0.38$. At the same time, the QF-fragments kinetic energy is about 15–20 MeV higher than that for the CN fission. The standard deviation of kinetic energy σ_{TKE} is 16 MeV that is smaller than σ_{TKE} expected for fission (22 MeV).

At the interaction energies of 250 and 284 MeV, the threshold for the fast fission process is overcome. According to the performed calculations, the contribution of this process at these interaction energies is significant and amounts to 39% and 61%, respectively. The mass-energy distributions of fast fission fragments at the energies of 250 and 284 MeV are characterized by a slight mass asymmetry $\eta \approx 0.22$. Contrary to LDM, the variance of TKE for fast fission decreases with increasing interaction energy. The comparison of the fast fission mass distribution with that obtained in the ^{12}C $+$ ^{238}U reaction, leading to the formation of the neighboring composite system ^{250}Cf at similar excitation energy $E^* \approx 100$ MeV, revealed the same positions of the asymmetric mass splits, whereas the entrance-channel mass asymmetry strongly varies (0.57 for ^{40}Ca $+$ ^{144}Sm and 0.90 for ^{12}C $+$ ^{238}U).

The analysis has shown that QF and fast fission have completely different characteristics of the mass-energy distributions. In the ^{40}Ca $+$ ^{208}Pb reaction, the QF fragments focus mainly around the closed neutron ($N = 50$) and proton ($Z = 28$) shells that apparently leads to an increase in TKE for this process compared to the CN fission. In the fast fission process no influence of known neutron or proton shells on the asymmetric mass distribution was found.

[1] Y. T. Oganessian and V. K. Uteonkov, Nucl. Phys. **A944**, 62 (2015).

[2] R. Bass, *Nuclear Reactions with Heavy Ions* (Springer-Verlag, Nrw York, 1980).

[3] M. G. Itkis, E. Vardaci, I. M. Itkis, G. N. Knyazheva, and E. M. Kozulin, Nucl. Phys. **A944**, 204 (2015).

[4] V. I. Zagrebaev and W. Greiner, Nucl. Phys. **A944**, 257 (2015).

[5] C. Simenel and A. Umar, Prog. Part. Nucl. Phys. **103**, 19 (2018).

[6] A. K. Nasirov, G. Mandaglio, G. Giardina, A. Sobiczewski, and A. I. Muminov, Phys. Rev. C **84**, 044612 (2011).

[7] C. Lebrun, F. Hanappe, J. F. Lecolley, F. Lefebvres, C. Ngô, J. Péter, and B. Tamain, Nucl. Phys. **A321**, 207 (1979).

[8] B. Borderie, M. Berlanger, D. Gardès, F. Hanappe, L. Nowicki, J. Péter *et al.*, Z. Phys. A: At. Nucl. **299**, 263 (1981).

[9] C. Gregoire, C. Ngô, and B. Remaud, Phys. Lett. B **99**, 17 (1981).

[10] C. Grégoire, C. Ngô, and B. Remaud, Nucl. Phys. A **383**, 392 (1982).

[11] C. Gregoire, C. Ngo, E. Tomasi, B. Remaud, and F. Scheuter, Nucl. Phys. A **387**, 37 (1982).

[12] C. Ngô, C. Gregoire, B. Remaud, and E. Tomasi, Nucl. Phys. **A400**, 259 (1983).

[13] Z. Zheng, B. Borderie, D. Gardes, H. Gauvin, F. Hanappe, J. Peter, M. F. Rivet, B. Tamain, and A. Zaric, Nucl. Phys. A **422**, 447 (1984).

[14] A. Van Geertruyden and Ch. Leclercq-Willain, Nucl. Phys. A **459**, 173 (1986); **459**, 196 (1986).

[15] A. J. Sierk, Phys. Rev. C **33**, 2039 (1986).

[16] V. Bernard, C. Gregoire, C. Mazur, C. Ngô, M. Ribrag, G. Y. Fan, P. Gonthier, H. Ho, W. Kühn, and J. P. Wurm, Nucl. Phys. A **385**, 319 (1982).

[17] H. Baba, N. Takahashi, A. Yokoyamaa, and T. Saito, Eur. Phys. J. A **3**, 281 (1998).

[18] G. N. Knyazheva, M. G. Itkis, S. V. Khlebnikov, E. M. Kozulin, V. G. Lyapin, V. A. Rubchenya, and W. Trzaska, Phys. Part. Nucl. Lett. **5**, 21 (2008).

[19] E. V. Prokhorova, A. A. Bogachev, M. G. Itkis, I. M. Itkis, G. N. Knyazheva, N. A. Kondratiev *et al.*, Nucl. Phys. A. **802**, 45 (2008).

[20] C. Simenel, D. J. Hinde, R. du Rietz, M. Dasgupta, M. Evers, C. J. Lin, D. H. Luong, and A. Wakhle, Phys. Lett. B **710**, 607 (2012).

[21] K. Banerjee, D. J. Hinde, M. Dasgupta, E. C. Simpson, D. Y. Jeung, C. Simenel, B. M. A. Swinton-Bland, E. Williams, I. P. Carter, K. J. Cook, H. M. David, Ch. E. Düllmann, J. Khuyagbaatar, B. Kindler, B. Lommel, E. Prasad, C. Sengupta, J. F. Smith, K. Vo-Phuoc, J. Walshe, and A. Yakushev, Phys. Rev. Lett. **122**, 232503 (2019).

[22] D. J. Hinde, M. Dasgupta, and E. C. Simpson, Prog. Part. Nucl. Phys. **118**, 103856 (2021).

[23] R. du Rietz, E. Williams, D. J. Hinde, M. Dasgupta, M. Evers, C. J. Lin, D. H. Luong, C. Simenel, and A. Wakhle, Phys. Rev. C **88**, 054618 (2013).

[24] R. Bass, Nucl. Phys. A **231**, 45 (1974).

[25] E. M. Kozulin, G. N. Knyazheva, K. V. Novikov, I. M. Itkis, M. G. Itkis, S. N. Dmitriev, Yu. Ts. Oganessian, A. A. Bogachev, N. I. Kozulina, I. Harca, W. H. Trzaska, and T. K. Ghosh, Phys. Rev. C **94**, 054613 (2016).

[26] H. J. Gils, H. Rebel, and E. Friedman, Phys. Rev. C **29**, 1295 (1984).

[27] J. Birkhan, M. Miorelli, S. Bacca, S. Bassauer, C. A. Bertulani, G. Hagen, H. Matsubara, P. von Neumann-Cosel, T. Papenbrock, N. Pietralla, V. Yu. Ponomarev, A. Richter, A. Schwenk, and A. Tamii, Phys. Rev. Lett. **118**, 252501 (2017).

[28] P. W. Wen, O. Chuluunbaatar, A. A. Gusev, R. G. Nazmitdinov, A. K. Nasirov, S. I. Vinitsky, C. J. Lin, and H. M. Jia, Phys. Rev. C **101**, 014618 (2020).

[29] V. I. Zagrebaev and V. V. Samarin, Phys. At. Nucl. **67**, 1462 (2004).

[30] A. V. Karpov, A. S. Denikin, M. A. Naumenko, A. P. Alekseev, V. A. Rachkov, V. V. Samarin, V. V. Saiko, and V. I. Zagrebaev, Nucl. Instrum. Methods Phys. Res., Sect. A **859**, 112 (2017).

[31] K. Hagino, N. Rowley, and A. T. Kruppa, Comput. Phys. Commun. **123**, 143 (1999).

[32] R. Graeger, D. Ackermann, M. Chelnokov, V. Chepigin, Ch. E. Düllmann, J. Dvorak, J. Even, A. Gorshkov, F. P. Heßberger, D. Hild, A. Hübner, E. Jäger, J. Khuyagbaatar, B. Kindler, J. V. Kratz, J. Krier, A. Kuznetsov, B. Lommel, K. Nishio, H. Nitsche, J. P. Omtvedt, O. Petrushkin, D. Rudolph, J. Runke, F. Samadani, M. Schädel, B. Schausten, A. Türler, A. Yakushev, and Q. Zhi, Phys. Rev. C **81**, 061601(R) (2010).

[33] A. V. Ignatyuk, M. G. Itkis, V. N. Okolovich, G. N. Smirenkin, and A. S. Tishin, Sov. J. Nucl. Phys. **21**, 612 (1975); A. V. Ignatyuk, G. N. Smirenkin, and A. S. Tishin, *ibid.* **21**, 255 (1975).

[34] V. Zagrebaev, A. Karpov, Y. Aritomo, M. Naumenko, and W. Greiner, Phys. Part. Nucl. **38**, 469 (2007).

[35] J. Maruhn and W. Greiner, Z. Phys. **251**, 431 (1972).

[36] S. Yamaji, H. Hofmann, and R. Samhammer, Nucl. Phys. A **475**, 487 (1988).

[37] E. M. Kozulin, A. A. Bogachev, M. G. Itkis, I. M. Itkis, G. N. Knyazheva, N. A. Kondratiev *et al.*, Instrum. Exp. Tech. **51**, 44 (2008).

[38] D. J. Hinde, M. Dasgupta, J. R. Leigh, J. C. Mein, C. R. Morton, J. O. Newton, and H. Timmers, Phys. Rev. C **53**, 1290 (1996).

[39] D. C. Hoffman, D. M. Lee, K. E. Gregorich, M. J. Nurmia, R. B. Chadwick, K. B. Chen, K. R. Czerwinski, C. M. Gannett, H. L. Hall, R. A. Henderson, B. Kadkhodayan, S. A. Kreek, and J. D. Leyba, Phys. Rev. C **41**, 631 (1990).

[40] M. G. Itkis and A. Ya. Rusanov, Phys. Part. Nucl. **29**, 160 (1998).

[41] J. R. Nix and W. J. Swiatecki, Nucl. Phys. **71**, 1 (1965).

[42] D. Hilscher and H. Rossner, Ann. Phys. (France) **17**, 471 (1992).

[43] I. I. Gonchar, Phys. Part. Nucl. **26**, 394 (1995).